PCCP

View Online / Journal Homepage
Dynamic Article Links

Cite this: DOI: 10.1039/c2cp42121f

www.rsc.org/pccp

PAPER

Desalination and hydrogen, chlorine, and sodium hydroxide production *via* electrophoretic ion exchange and precipitation†

Viktor Shkolnikov, Supreet S. Bahga and Juan G. Santiago*

Received 5th April 2012, Accepted 28th June 2012
DOI: 10.1039/c2cp42121f

We demonstrate and analyze a novel desalination method which works by electrophoretically replacing sodium and chloride in feed salt water with a pair of ions, calcium and carbonate, that react and precipitate out. The resulting calcium carbonate precipitate is benign to health, and can be filtered or settled out, yielding low ionic strength product water. The ion exchange and precipitation employs self-sharpening interfaces induced by movement of multiple ions in an electric field to prevent contamination of the product water. Simultaneously, the electrolysis associated with the electromigration produces hydrogen gas, chlorine gas, and sodium hydroxide. We conducted an experimental study of this method's basic efficacy to desalinate salt water from 100 to 600 mol m^{-3} sodium chloride. We also present physicochemical models of the process, and analyze replacement reagents consumption, permeate recovery ratio, and energy consumption. We hypothesize that the precipitate can be recycled back to replacement reagents using the well-known, commercially implemented Solvay process. We show that the method's permeate recovery ratio is 58% to 46%, which is on par with that of reverse osmosis. We show that the method's energy consumption requirement over and above that necessary to generate electrolysis is 3 to 10 W h l^{-1}, which is on par with the energy consumed by state-of-the-art desalination methods. Furthermore, the method operates at ambient temperature and pressure, and uses no specialized membranes. The process may be feasible as a part of a desalination-co-generation facility: generating fresh water, hydrogen and chlorine gas, and sodium hydroxide.

1. Introduction

Fresh water and energy availability are among the top few most important technological issues facing the world. Population growth and improved standard of living, together with increased agricultural and industrial activities further limit the availability of these two resources. The United Nations Population Fund (UNPF) estimated in 2001 that the world used 54% of annual available fresh water.[1] UNPF further estimates that by 2025 the world will use 70% of annual available fresh water, due to population growth alone.[1] This water scarcity can be mitigated through both consumption reduction and supply increase through efficient and practical water purification and desalination technologies. Currently, reverse osmosis (RO), multistage flash distillation (MSF), and electrodialysis (ED) comprise roughly 44%, 40%, and 6% of world desalination production capacity, respectively.[2] Of these, MSF is least energy efficient[3] but uses less expensive thermal energy, so it is used where fuel is relatively inexpensive.[2] RO and ED are more energy efficient[3] but require more expensive electrical energy and special membranes. Membranes can constitute significant process cost, are prone to fouling, and require frequent replacement.[2,4,5]

One way to perform desalination and avoid costs associated with special membranes, high temperature, and high pressure is to perform desalination using ion exchange. Since the beginning of the 20th century, ion exchange between solid and liquid phases has been used for water softening, recovery of metals from aqueous solutions, and production of high purity water for specialty applications (*e.g.*, boilers).[6] Weiss reviews some of these early attempts, including pilot plants for desalinating brackish water *via* ion exchange.[7] Modern attempts at desalination *via* ion exchange center around desalination of oil and natural gas byproduct waters.[8,9] Desalination of sea water *via* ion exchange has been proposed employing ammonium salts combined with distillation[6] or precipitation.[10] For example, Glueck proposed combining the basic processes of ion exchange between solid and liquid phases and precipitation to achieve desalination.[10] Glueck suggested passing feed water through a cationic exchanger presaturated with silver ions. As silver ions react with chloride ions to form silver chloride precipitate, chloride ions are removed from the feed water. Meanwhile the ion exchange

Department of Mechanical Engineering, Stanford University, Stanford, CA 94305, USA. E-mail: juan.santiago@stanford.edu; Fax: +1 650-723-5689; Tel: +1 650-723-7657
† Electronic supplementary information (ESI) available. See DOI: 10.1039/c2cp42121f

resin takes up the sodium, thus yielding product water. The resin is regenerated by passing ammonia solution through the precipitate, forming a diaminosilver complex, and then heating the complex in the presence of the resin, generating waste brine. The major drawback of methods employing ion exchange between solid and liquid phases is the requirement for the solid ion exchange material as well as the replacement ions, each expensive materials needing periodic replacement.

We here propose a novel method which combines purely liquid-phase ion exchange *via* electrophoresis with precipitation to desalinate brackish and sea water. We leverage an electric current and differences in associated ion mobilities to effect self-sharpening interfaces which spatially confine and help prevent contamination of the product water. The approach avoids drawbacks associated with ion exchange resins and specialty membranes. We present a version which exchanges chloride ions for carbonate ions and sodium ions for calcium ions. Carbonate ions quickly react with calcium ions to form calcium carbonate (limestone) precipitate, which we remove, producing fresh water. We hypothesize that calcium carbonate can be recycled back into the replacement reagents using the Solvay process.[11] Our method requires electrolysis to sustain current and so generates hydrogen and chlorine gases and sodium hydroxide due to electrode reactions. We therefore envision that this method may be useful as part of a co-generation facility: generating fresh water, hydrogen gas, chlorine gas, and sodium hydroxide. We offer here a study in which we demonstrate the basic efficacy of the processes experimentally and develop a theoretical framework to analyze the method.

We first describe the method conceptually and then develop models for the method's reagent consumption, permeate recovery ratio, and energy consumption. We discuss theoretical optimization of device geometry to minimize energy consumption, and compare this theoretical estimate with the energy consumption of state-of-the-art desalination methods. Finally, we experimentally demonstrate basic desalination and experimentally validate key aspects of the model. The results suggest that the method's permeate recovery ratio and non-recoverable energy consumption can be theoretically on par with that of state-of-the-art desalination methods. The method operates at ambient temperature and pressure and requires no specialized membranes.

2. Concept and theory

2.1 Method concept

We developed a technique to remove ions from salt water by electrophoretically exchanging sodium and chloride in feed salt water with a cation and an anion which react with each other and precipitate out, creating low ionic strength product water. We term this technique as electrophoretic precipitative desalination (EPD). The EPD scheme that we investigate in detail involves exchanging chloride ions for carbonate ions and sodium ions for calcium ions. Carbonate ions then react with calcium ions to form calcium carbonate (limestone) precipitate, which can be settled or filtered out, producing fresh water.

Fig. 1 is a schematic representation of our desalination concept. To remove chloride ions in feed water, we place the

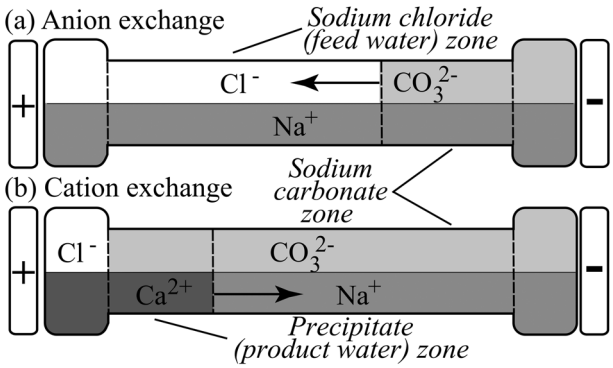

Fig. 1 Schematic illustrating electrophoretic precipitative desalination in a simple channel terminating in two reservoirs. We first exchange chloride ions in feed water with carbonate ions. Next, we exchange sodium ions for calcium ions, and form calcium carbonate. Arrows indicate the motion of interfaces. Dashed lines delimitate the sodium chloride (feed water), sodium carbonate, and precipitate (product water) zones. In the first step (a), under applied electric field, carbonate ions trail higher mobility chloride ions, forming a sharp boundary between the sodium chloride (feed water) zone and sodium carbonate zone. After this boundary reaches the anode (left) reservoir, we empty this reservoir and fill with calcium chloride solution. (b) We again apply an electric field, and calcium ions trail higher mobility sodium ions forming a sharp boundary between the sodium carbonate and precipitate (product water) zones. As calcium ions meet carbonate ions they form calcium carbonate precipitate, yielding low ionic strength product water.

feed salt water into an anode reservoir and a channel or chamber which connects to a cathode reservoir. We then fill the cathode reservoir with sodium carbonate solution (Fig. 1a), and apply an electric current. Chloride ions electromigrate towards the anode followed by lower electrophoretic mobility carbonate ions. The difference in electrophoretic mobility causes a self-sharpening ion concentration shock wave between the leading chloride ions and the trailing carbonate ions. This wave is similar to those observed in isotachophoresis (ITP).[12,13] As in ITP, the sodium carbonate concentration in the channel is governed in part by the original sodium chloride concentration of the channel, in accordance with current continuity and local electroneutrality in each zone.

Once the channel is filled with sodium carbonate we proceed to exchange the cations. We replace the contents of the anode reservoir with calcium chloride solution and again apply an electric field as shown in Fig. 1b. At the ionic strengths of interest, the leading sodium ions have electrophoretic mobility larger than that of calcium ions. Therefore, calcium ions trail the higher mobility sodium ions. Concurrently, the calcium ions react with the counter-migrating carbonate ions to form calcium carbonate:

$$Ca^{2+} + CO_3^{2-} \rightarrow CaCO_3 \qquad (1)$$

This leads to a growing calcium carbonate (product water) zone, again bounded by a sharp boundary between the sodium and calcium ion regions. Calcium carbonate precipitates out of solution, leaving behind low ionic strength solution containing calcium, carbonate, and bicarbonate ions, and possibly other solutes (*e.g.*, very low or zero mobility contaminant species)

that have not been exchanged. We then recover the contents of the precipitate zone and remove the precipitate, keeping the fresh water. As precipitated calcium carbonate occupies less than about 1% of the channel volume (as discussed in Section 2.3), the volume of fresh water produced is essentially equal to the volume of the solution recovered.

2.2 Choice of replacement ions

We recommend choosing replacement ions based on the solubility product of the resulting precipitate, their electrophoretic mobility, their adverse health effects, and their cost. The replacement anions and cations need to react to form a salt with solubility equilibrium concentrations on the order of the ionic strength of the desired fresh water[14] (order 8 mol m^{-3}). Product water ionic strength can likely be as low as needed, as lowering of product water ionic strength slightly lowers the energy consumption (see Section 2.6.4). The replacement anions and cations should have electrophoretic mobilities lower than those of chloride and sodium, respectively, to enable self-sharpening interfaces between zones and minimize inter-zone mixing. In accordance with these criteria, we here chose to investigate calcium and carbonate as replacement ions.

Another concern is the presence of ions other then sodium and chloride in the feed water. For example, sea and brackish water may also contain bicarbonate, sulfate, calcium, magnesium, barium, and strontium ions.[2] We hypothesize that using calcium and carbonate as replacement ions, calcium and bicarbonate will remain in the precipitate (product water) and the sodium carbonate zones, respectively. Further, sulfate ion concentration will likely be reduced by reaction with calcium to form calcium sulfate precipitate. Concentrations of magnesium, barium, and strontium will likely be reduced due to reactions with carbonate.

2.3 Model for ion concentration profiles and interface velocities

The ion concentrations in the process, including those of the product water, are governed by electrophoretic migration, bulk charge neutrality of the zones, acid–base reactions, and precipitation reactions. During anion exchange, the leading (sodium chloride) zone migrates towards the anode, followed by a growing trailing (sodium carbonate) zone, as depicted in Fig. 1a. The composition of the leading zone does not change during migration. Knowing the composition of the leading zone, we can calculate the composition of the trailing zone, using the electrophoretic migration equation[15] integrated in space and time across the interface between the two zones as follows:

$$(c_{i,\mathrm{L}} - c_{i,\mathrm{T}})\frac{\Delta x}{\Delta t} = j\left(\frac{\mu_{i,\mathrm{L}}c_{i,\mathrm{L}}}{\sigma_{\mathrm{L}}} - \frac{\mu_{i,\mathrm{T}}c_{i,\mathrm{T}}}{\sigma_{\mathrm{T}}}\right), \qquad (2)$$

where $c_{i,\mathrm{L}}$ and $c_{i,\mathrm{T}}$ are the concentration of species i in the leading and trailing zones, respectively; $\mu_{i,\mathrm{L}}$ and $\mu_{i,\mathrm{T}}$ are the electrophoretic mobilities of species i in the leading and trailing zones, respectively; σ_{L} and σ_{T} are the local conductivity of the leading and trailing zones, respectively; $\Delta x/\Delta t$ is the velocity of the interface; and j is the current density. In our notation the first subscript denotes the species of interest; the second subscript denotes the zone. Eqn (2) is similar to the Rankine–Hugoniot jump conditions for supersonic shock waves in compressible fluid mechanics,[16] and serves here to describe ion concentration shock waves. We find the velocity of the interface by noting that the leading zone contains only the higher mobility ion and its counter ion, so eqn (2) for either the anion or the cation of the leading zone (L) (for anion and cation exchange respectively) simplifies to:

$$\frac{\Delta x}{\Delta t} = \frac{j\mu_{i,\mathrm{L}}}{\sigma_{\mathrm{L}}}. \qquad (3)$$

For anion exchange, we find the composition of the sodium carbonate zone by solving eqn (2) for sodium, chloride, and carbonic acid ions together with the equations for carbonic acid equilibrium and local charge neutrality ($\sum_i z_i c_i = 0$, where z is the valance) in each zone. We neglect the contribution of hydrogen and hydroxyl ions to electroneutrality and zone resistivity.[17] We expect hydrogen and hydroxyl ion concentrations to be significantly less than those of sodium, chloride or carbonic acid ions. We incorporate the dependence of electrophoretic mobility on ionic strength using a custom numerical solver we wrote together with the electrophoresis simulator SPRESSO written in MATLAB.[18,19] These calculations show that the sodium and total concentration (*i.e.*, all ionic states) of carbonic acid increases approximately linearly with increasing feed water concentration. We discuss these calculations further in the ESI.†

For the cation exchange, the leading zone is the sodium carbonate zone, and the trailing zone is formed by calcium migration and precipitation with carbonic acid (see Fig. 1b). This zone's composition is thus governed by calcium carbonate solubility, carbonic acid equilibrium, bulk net neutrality, and species conservation. Species conservation dictates that the net amount of calcium and carbonic acid that have entered the growing trailing zone must equal the amount of calcium and carbonic acid in all species remaining in this growing control volume (trailing zone). Calcium species remaining in the trailing zone include calcium carbonate and free calcium ions. Carbonic acid species remaining in the control volume include free carbonate and bicarbonate ions, dissolved carbon dioxide and calcium carbonate. We can express the conservation relations as follows:

$$c_{\mathrm{Ca,EN}} = c_{\mathrm{Ca^{2+}}} + c_{\mathrm{CaCO_3(s)}} \qquad (4)$$

$$c_{\overline{\mathrm{H_2CO_3}},\mathrm{EN}} = c_{\mathrm{CO_3^{2-}}} + c_{\mathrm{HCO_3^-}} + c_{\mathrm{CO_2}} + c_{\mathrm{CaCO_3}(s)} - c_{\mathrm{CO_2,OR}}, \qquad (5)$$

where, $c_{\mathrm{Ca,EN}}$ and $c_{\overline{\mathrm{H_2CO_3}},\mathrm{EN}}$ are the net moles of calcium and carbonic acid, respectively, which have entered the growing trailing zone per final volume of the trailing zone; $c_{\mathrm{Ca^{2+}}}$ is the concentration of free calcium ions; and $c_{\mathrm{CO_3^{2-}}}$ and $c_{\mathrm{HCO_3^-}}$ are the concentrations of the free carbonate and bicarbonate ions, respectively. Further, $c_{\mathrm{CO_2}}$ is the concentration of dissolved carbon dioxide in the water; $c_{\mathrm{CO_2,OR}}$ is the concentration of dissolved carbon dioxide originally present in the water (*e.g.*, due to equilibrium with the local atmosphere) before the trailing zone existed; and $c_{\mathrm{CaCO_3(s)}}$ is the moles of solid calcium carbonate per final volume of the trailing zone.

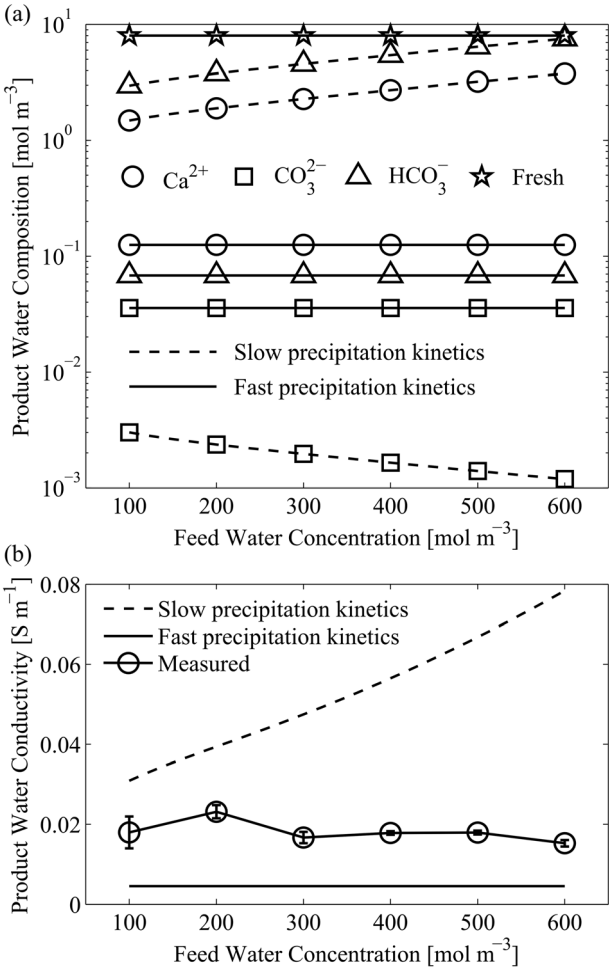

Fig. 2 Predictions of product water composition (a) and predictions and measurements of product water conductivity (b) for feed water concentrations from 100 to 600 mol m^{-3} sodium chloride. The product water is assumed to contain calcium (○), carbonate (□), and bicarbonate (△) ions. We show also the limit[14] for fresh water of 8 mol m^{-3} (☆). In the case of slow precipitation kinetics (large precipitation-to-electromigration time scale ratio) (dashed lines), we predict the concentrations of calcium and bicarbonate in the product water zone (and associated conductivity) to be high, but still below the fresh water limit. Further, we predict product water ionic strengths and conductivity to increase with feed water concentration. For the case of fast precipitation kinetics (solid lines), the concentrations of calcium and bicarbonate in the product water zone are low, and the ionic strengths and conductivity of the product water are correspondingly low and approximately independent of feed water concentration. In the bottom plot, we show measured product water conductivity from our experiments. The measurements are bounded by the two limiting cases, suggesting that the precipitation time scales were roughly on the same order as the electromigration timescales. These measurements also confirm that we can desalinate feed water concentrations of 100 to 600 mol m^{-3}.

Since calcium carbonate is uniformly distributed throughout the trailing zone, $c_{CaCO_3(s)}$ may be interpreted as the system-averaged molar density of the solid precipitate. The overbar on carbonic acid concentration refers to the total concentration of carbonic acid derivatives: carbonate, bicarbonate, and carbonic acid. The subscripts EN and OR denote "entered" and "originally present".

The amount of calcium and carbonic acid that enters the trailing zone depends on the relative time scales of the precipitation reaction *versus* the time scale of electromigration into the trailing zone. The relative dynamics of these are not known, so we here consider two extreme cases. For relatively fast electromigration, $c_{Ca,EN}$ and $c_{\overline{H_2CO_3},EN}$ are given by eqn (2) together with the equations for carbonic acid equilibrium and local electroneutrality in each zone. Accordingly, we can estimate these concentrations in a manner similar to that used above to calculate the composition of the trailing zone in anion exchange. If, on the other hand, precipitation kinetics are relatively fast, then the precipitation reaction quickly establishes conditions behind the shock. In this case, we assume that the trailing zone composition instantly reaches the equilibrium composition, and we obtain $c_{Ca,EN}$ and $c_{\overline{H_2CO_3},EN}$ from the corresponding net flux of these species into the trailing zone:

$$c_{Ca,EN} = \left(\frac{c_{Ca^+}\mu_{Ca^+,\infty}}{\sigma_{ppt}}\right)\frac{\sigma_{Na^+/\overline{H_2CO_3}}}{\mu_{Na^+,Na^+/\overline{H_2CO_3}}}, \tag{6}$$

$$c_{\overline{H_2CO_3},EN} = \left(\frac{c_{\overline{H_2CO_3},Na^+/\overline{H_2CO_3}}\mu_{\overline{H_2CO_3},Na^+/\overline{H_2CO_3}}}{\sigma_{Na^+/\overline{H_2CO_3}}} - \frac{c_{CO_3^{2-}}\mu_{CO_3^{2-},\infty} + c_{HCO_3^-}\mu_{HCO_3^-,\infty}}{\sigma_{ppt}}\right) \times \frac{\sigma_{Na^+/\overline{H_2CO_3}}}{\mu_{Na^+,Na^+/\overline{H_2CO_3}}}. \tag{7}$$

Here $\mu_{Ca^+,\infty}$, $\mu_{CO_3^{2-},\infty}$ and $\mu_{HCO_3^-,\infty}$ are the electrophoretic mobilities of calcium, carbonate, and bicarbonate, respectively, at infinite dilution; $\mu_{Na^+,Na^+/\overline{H_2CO_3}}$ is the electrophoretic mobility of sodium in the sodium carbonate zone; $\mu_{\overline{H_2CO_3},Na^+/\overline{H_2CO_3}}$ is the net effective electrophoretic mobility of carbonic acid derivatives in the sodium carbonate zone (again the overbar refers to the sum of all carbonic acid derivatives); $c_{\overline{H_2CO_3},Na^+/\overline{H_2CO_3}}$ is the total concentration of carbonic acid derivatives in the sodium carbonate zone; σ_{ppt} and $\sigma_{Na^+/\overline{H_2CO_3}}$ are the conductivity of the precipitate and the sodium carbonate zones, respectively (see Fig. 1). To estimate the trailing zone composition, we simultaneously solve eqn (4) through (7) together with the equations for carbonic acid equilibrium and calcium carbonate solubility equilibrium and local electroneutrality in each zone (for details see ESI†).

Since the relative time scale of precipitation is not known, we here propose to bound the composition of the cation exchange trailing zone between the two limiting cases described above: for relatively slow and fast precipitation kinetics relative to the electromigration time scale. We show solutions under these two assumptions for the concentrations of sodium, carbonate, and bicarbonate ions in the cation exchange trailing zone in Fig. 2a for feed water concentrations from 100 to 600 mol m^{-3} sodium chloride. As a reference, we also plot the maximum allowable ionic concentration for still considered fresh water (8 mol m^{-3}, as per ref. 14). The assumption of fast precipitation kinetics (solid lines) leads to lower predicted ion

concentrations in the trailing zone. Also, for relatively slow precipitation kinetics (dashed lines), the predicted trailing (product water) zone concentrations are higher, but are still below the maximum allowable level of fresh water concentration. For this case, a stronger dependence on electromigration fluxes results in a final ionic strength which increases with increasing feed water concentration. Fig. 2b shows associated plots of the predicted conductivity of the cation exchange trailing (product water) zone as a function of the concentration of the feed water zone. Again, fast precipitation kinetics leads to low product water conductivity, while slow precipitation yields significantly higher conductivity. We shall later compare these predictions with the experimental data also shown in Fig. 2b. For now, we stress that, for either assumption, we expect the maximum product water zone concentration to be well below the requirement for fresh water.

Lastly, we can calculate the expected moles of solid calcium carbonate per final volume of the trailing zone, $c_{CaCO_3(s)}$, for feed water concentrations of 100 to 600 mol m^{-3} sodium chloride. These concentrations range from 43.5 to 221 mol m^{-3} for the slow precipitation kinetics case and from 32.9 to 176 mol m^{-3} for the fast precipitation kinetics case. For all cases the precipitate occupies less than 1% of the channel volume (for details see ESI†). Thus, we will neglect the volume contribution of the solid precipitate.

2.4 Reagent consumption

During EPD, calcium chloride and sodium carbonate are consumed as calcium carbonate is produced. (Calcium chloride and sodium carbonate can likely be regenerated from calcium carbonate, as we discuss in Section 5.2.) The reagent consumption estimates follow from global equalities resulting from simple control volume analyses. Namely, the moles of sodium carbonate consumed are equal to the net moles of carbonic acid species which enter the channel in anion exchange and cation exchange steps; and the moles of calcium chloride consumed are equal to the moles of carbonic acid species consumed since calcium carbonate is formed. In turn, the moles of total carbonic acid species that enter the channel in anion exchange per volume of the channel is the concentration of total carbonic acid species in the trailing zone of anion exchange (see Fig. 1). Further, the moles of carbonate ions per volume of the channel that enter the channel in cation exchange is equal to the flux of carbonate ions times the product of the area of the channel and the known time for cation exchange. We summarize these calculations in Fig. S2 of the ESI†. For feed water ionic strength between 100 to 600 mol m^{-3}, the amount of calcium chloride consumed per volume of product water produced increases monotonically from 12 to 86 kg m^{-3}, and the amount of sodium carbonate consumed increases monotonically from 12 to 82 kg m^{-3}.

2.5 Maximum permeate recovery ratio

Permeate recovery ratio (PRR) is the ratio of the amount of product water produced to the amount of feed water consumed. One way to calculate PRR for this method is to assume that calcium carbonate is recycled to aqueous calcium chloride and sodium carbonate (as we discuss in Section 5.2) and so no product water is consumed to produce respective reservoir solutions. Hence, the net volume of product water produced would be the volume of the channel. However, to be conservative, we will not assume such a recycling process here. Instead, we will estimate the net volume of product water as the volume of the channel minus the volumes of the sodium carbonate reservoir and the calcium chloride reservoir. This conservative estimate assumes that product water from an earlier desalination batch was used to make the necessary sodium carbonate and calcium chloride solutions from solid reagents. The volume of feed water consumed would then be the volume of the channel and that of the sodium chloride reservoir.

The minimum volume of the sodium chloride reservoir is governed by the concentration of feed water and the amount of sodium chloride which migrates out of that reservoir. Likewise, the minimum volume of the sodium carbonate and calcium chloride reservoirs is dictated by the solubility limit of sodium carbonate and calcium chloride and the amount of sodium carbonate and calcium chloride consumed per volume of channel, respectively. Combining these estimates, the permeate recovery ratio, PRR, is given by

$$\begin{aligned} \mathrm{PRR} = & \left[1 - c_{\overline{H_2CO_3},Na^+/\overline{H_2CO_3}} \left(1 + \frac{\left|\mu_{\overline{H_2CO_3},Na^+/\overline{H_2CO_3}}\right|}{\left|\mu_{Na^+,Na^+/\overline{H_2CO_3}}\right|}\right) \right. \\ & \left. \times \left(\frac{1}{c_{CaCl_2,Max}} + \frac{1}{c_{Na_2CO_3,Max}}\right)\right] \\ & \times \left[1 + \frac{\left|\mu_{Na^+,NaCl}\right|}{\left|\mu_{Cl^-,NaCl}\right|}\right]^{-1}, \end{aligned} \tag{8}$$

where, $c_{CaCl_2,Max}$ and $c_{Na_2CO_3,Max}$ are, respectively, the maximum soluble concentrations of calcium chloride and sodium carbonate; $\mu_{Na^+,NaCl}$ and $\mu_{Cl^-,NaCl}$ are, respectively, the electrophoretic mobilities of sodium and chloride in the sodium chloride zone (see Fig. 1). $c_{\overline{H_2CO_3},Na^+/\overline{H_2CO_3}}$ is the total concentration of carbonic acid derivatives in the sodium carbonate zone, which varies approximately linearly with feed water concentration. Hence, the estimated PPR varies roughly linearly from 58% to 46% as feed water concentration varies from 100 to 600 mol m^{-3} sodium chloride (for details see ESI†). In comparison, typical permeate recovery ratio for sea water reverse osmosis is around 30% to 50%.[20]

2.6 Energy consumption and hydrogen gas, chlorine gas, and sodium hydroxide production

To analyze the energy consumption of electrophoretic precipitative desalination, we separate the total energy consumption into contributions due to reversible energy for electrode reactions, energy loss associated with activation overpotentials at the electrodes, and ohmic energy loss in the channel. We discuss these below.

2.6.1 Energy consumption due to oxidation–reduction reactions. At the anode, chloride ions are oxidized to chlorine gas, and at the cathode water is reduced to hydrogen gas and sodium hydroxide is generated. These reactions require at least

a reversible standard potential of about −2.19 V or 210 kJ per mole of electrons.[21] We obtain the amount of charge moved through the system in anion and cation exchange from fluxes of individual ions (for details see ESI†). From this we obtain that the ideal energy consumption due to electrode reactions per volume of the channel is

$$\frac{E_{rxn}}{V_c} = e_{rev}\left(2c_{NaCl} + c_{\overline{H_2CO_3},Na^+/\overline{H_2CO_3}}\frac{\left|\mu_{\overline{H_2CO_3},Na^+/\overline{H_2CO_3}}\right|}{\left|\mu_{Na^+,Na^+/\overline{H_2CO_3}}\right|}\right), \quad (9)$$

where e_{rev} is the reversible energy per mole of electrons moved through the system (here 210 kJ mole^{-1}), and c_{NaCl} is the concentration of feed water. $c_{\overline{H_2CO_3},Na^+/\overline{H_2CO_3}}$, the total concentration of carbonic acid derivatives in the sodium carbonate zone, varies approximately linearly with feed water concentration. Thus, the energy consumption due to electrode reactions increases roughly linearly with feed water concentration and is insensitive to device geometry and current density.

In addition, the system is expected to have energy loss due to activation overpotentials. This depends strongly on electrode material and geometry.[22] We discuss the contribution of overpotentials to the overall energy consumption, in detail, for platinum, graphite, and nickel electrodes in Section S6 in ESI.† We show that this contribution can be made negligible and thus we do not discuss it further here.

2.6.2 Hydrogen gas, chlorine gas, and sodium hydroxide production. We can relate the amount of hydrogen gas, chlorine gas, and sodium hydroxide produced to the amount of total charge used. As chloride ions are oxidized to chlorine gas, and water is reduced to hydrogen gas and hydroxide, 1 mol of each species is produced per 2 mol of charge moved through the system. Since, the amount of hydrogen, chlorine, and hydroxide produced is proportional to the amount of charge passed through the system, the amount produced increases roughly linearly with feed water concentration and is independent of device geometry or current density, similarly to energy consumption due to electrode reactions. Per volume of product water, we estimate EPD produces from 0.11 to 0.63 moles l^{-1} of hydrogen gas, chlorine gas, and sodium hydroxide for feed water sodium chloride concentrations of 100 to 600 mol m^{-3}.

2.6.3 Energy consumption due to ohmic losses. Flowing an electric current through an electrolyte causes ohmic energy consumption. We assume that the electrodes reside at the system boundaries (the outer boundaries of the reservoirs). Thus ohmic energy consumed during each step of EPD can be estimated as,

$$E_{ohm} = \int_0^{t_H} I^2 R \mathrm{d}t, \quad (10)$$

where t_H is the time for the interface between two zones to traverse the channel with length H, I is the applied current, and R is the resistance of the channel. We maintain a constant current in the channel so resistance is the only function of time. The resistance of the channel is proportional to the sum of the zone lengths divided by conductivity of each zone and channel cross sectional area. Using the interface velocity eqn (3) and assuming the channel length H is significantly larger than either of the zone interface widths, we obtain that the energy consumption for each of the two ion exchange steps as

$$E_{ohm} = \int_0^H I^2\left[\frac{x}{\sigma_T A} + \frac{H-x}{\sigma_L A}\right]\left(\frac{A\sigma_L}{I\mu_L}\right)\mathrm{d}x. \quad (11)$$

Here A is the channel cross sectional area, and μ_L is the electrophoretic mobility of the chloride ion in the sodium chloride zone for the anion exchange step and the mobility of the sodium ion in the sodium carbonate zone for cation exchange step. Evaluating the integral in eqn (11) and dividing by the volume of the channel yields an expression for ohmic energy consumption per volume of product water during each step:

$$\frac{E_{ohm}}{V_c} = \frac{jH}{2\mu_L}\left(1 + \frac{\sigma_L}{\sigma_T}\right), \quad (12)$$

where j is the local current density equal to I/A. The total ohmic energy consumption per volume of product water is then the sum of the energy per volume contributions of the anion and cation exchange steps:

$$\frac{E_{ohm}}{V_c} = \frac{jH}{2}\left[\frac{1}{\mu_{Cl^-,NaCl}}\left(1 + \frac{\sigma_{NaCl}}{\sigma_{Na^+/\overline{H_2CO_3}}}\right) + \frac{1}{\mu_{Na^+,Na^+/\overline{H_2CO_3}}}\left(1 + \frac{\sigma_{Na^+/\overline{H_2CO_3}}}{\sigma_{ppt}}\right)\right]. \quad (13)$$

Here σ_{NaCl} is the conductivity of the sodium chloride (feed water) zone. Ohmic energy consumption per volume of the channel is therefore proportional to current density and the length of the channel and depends on feed water concentration through specific zone conductivities. In Fig. 3, we plot the ohmic energy consumption scaled by channel volume, effective channel length, and current density as a function of feed water sodium chloride concentrations ranging from 100 to 600 mol m^{-3} sodium chloride for the cases of small (solid lines) and large (dashed lines) precipitation-to-migration time scale ratios. In both regimes, ohmic energy consumption increases with feed water concentration. For fast precipitation kinetics, the conductivity of the cation exchange trailing zone (precipitate zone) is lower and so we predict greater ohmic losses. In both cases, the conductivity of the precipitate zone is much smaller than that of the sodium chloride or sodium carbonate zones (the second term in parenthesis in eqn (13)). Therefore, the precipitation (cation exchange) step dominates the net ohmic energy consumption.

2.6.4 Minimizing ohmic energy consumption. We here formulate an estimate for minimum energy loss in EPD. Earlier, we showed ohmic energy consumption per channel volume is proportional to current density and channel length. This result assumed that the channel length (distance between the electrodes) H was significantly larger than the widths of the zone interfaces. As we consider lowering of both current

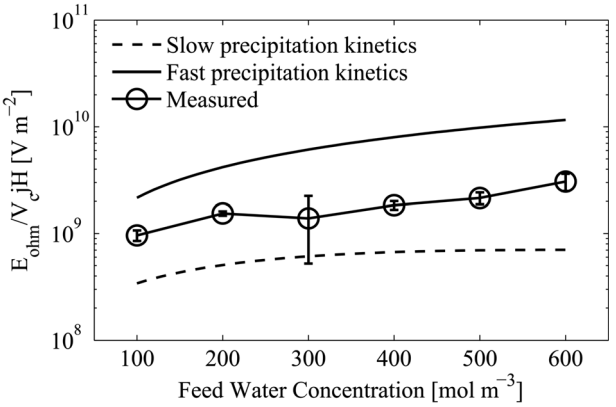

Fig. 3 Comparison of predictions and measurements of ohmic energy consumption normalized by the product of the channel volume, current density, and channel length for feed water concentrations of 100 to 600 mol m^{-3} sodium chloride. The experiments were performed at current densities ranging between 0.72 and 53 kA m^{-2} (for details see Section S10 of ESI†). Uncertainty bars on measurements represent 95% confidence on the mean (respectively, there are N = 4, 6, 4, 7, 6, and 6 repetitions for the measurements from 100 to 600 mol m^{-3}). For the case of slow precipitation kinetics (large precipitation-to-migration time scale ratio) (dashed lines) the ohmic energy consumption is roughly an order of magnitude smaller than that for the case of fast precipitation kinetics (small precipitation-to-migration time scale ratio) (solid lines). The cation exchange step contributes much more to ohmic energy consumption than the anion exchange step, and this energy consumption is roughly inversely proportional to product water conductivity (see eqn (13) in the text). For the slow precipitation kinetics, we predict higher product water conductivity then for fast precipitation kinetics (see Fig. 2). Thus, ohmic energy consumption for fast precipitation kinetics case is higher. The two sets of predictions bracket the measured ohmic energy consumption values. As in the cases of fast and slow precipitation kinetics, the measured ohmic energy consumption increases with feed water concentration.

density and channel length, we explore the expected interface widths in more detail and compare these to the minimum length of the distance between electrodes.

For the anion exchange step, we estimate the width of the interface employing the theory of MacInnes and Longsworth[23] for diffusion-limited interfaces between disparate anions (see also Garcia-Schwarz *et al.*[24]). Following MacInnes and Longsworth, we define the interface width as the distance for the ratio of chloride concentration to the square root of total concentration of carbonic acid derivatives to change from unity to exp(1). Thus the anion exchange interface width, w_{an}, is given by

$$w_{an} \approx \frac{1}{j}\left(\frac{kT}{e}\right)\frac{\sigma_{NaCl}\mu_{\overline{H_2CO_3},Na^+/\overline{H_2CO_3}}}{(\mu_{Cl^-,NaCl}-\mu_{\overline{H_2CO_3},Na^+/\overline{H_2CO_3}})}, \qquad (14)$$

where k is Boltzmann's constant, T is the temperature, and e is the elementary charge. We see the anion exchange interface width scales inversely with the current density. Similarly, for the cation exchange, we employ a scaling argument equating diffusive and electrophoretic fluxes at the interface. Here, we define the interface width as the distance for the concentration of the leading ion (sodium) to change from 90% to 10% of its concentration in the leading zone (sodium carbonate zone). Hence, we obtain a similar estimate for the cation exchange zone width w_{cat}:

$$w_{cat} \approx \frac{4}{5}\frac{1}{j}\left(\frac{kT}{e}\right)\sigma_{ppt}. \qquad (15)$$

We see that the cation exchange interface width also scales inversely with the current density (for more details regarding these width estimates, see ESI†). We conclude that current density and channel length can be reduced, but channel length should be significantly larger than interface widths.

Now, for a practical apparatus, we may expect that the minimum length between the electrodes (channel length) to be at least a few times larger than the widths of ion zone interfaces. To estimate the minimum ohmic energy consumption, we here set the channel length for anion and cation exchange to be 5 times the interface width for anion and cation exchange steps, respectively. In a simple one-dimensional setup like that depicted in Fig. 1, this would yield product water from roughly 80% of the channel. Thus, combining eqn (14) and (15) with eqn (13), we obtain the following estimate for minimum ohmic energy consumption per volume of the channel:

$$\min\left(\frac{E_{ohm}}{V_c}\right) \approx \frac{5}{2}\left(\frac{kT}{e}\right)\left\{\sigma_{NaCl}\left[\frac{\mu_{\overline{H_2CO_3},Na^+/\overline{H_2CO_3}}}{\mu_{Cl^-,NaCl}\left(\mu_{Cl^-,NaCl}-\mu_{\overline{H_2CO_3},Na^+/\overline{H_2CO_3}}\right)}\left(1+\frac{\sigma_{NaCl}}{\sigma_{Na^+/\overline{H_2CO_3}}}\right)\right]\right\}. \qquad (16)$$

We see this estimate of minimum total ohmic energy consumption scales superlinearly with feed water concentration and is independent of device geometry or current density. The term within the square brackets varies slowly with feed water concentration. Also, the conductivity of the sodium carbonate zone is roughly proportional to the conductivity of the feed water zone, and each is usually much greater than the conductivity of the precipitate zone. Therefore, the minimum total ohmic energy consumption per volume roughly scales with conductivity of the feed water zone, and thus with the concentration of feed water. Furthermore, from the second term in curly brackets in eqn (16), the larger the conductivity of the precipitate zone, the larger the minimum total ohmic energy consumption per volume. Thus it is desired to have conductivity of the product water zone to be as low as practical. In other words, the solubility product of replacement ions should be as low as practical. This maintains high field in the product water zone and associated thin interface width for the cation exchange. We plot this hypothetical minimum ohmic energy estimate as a function of feed water concentration in the range of 100 to 600 mol m^{-3} sodium chloride in Fig. 4 (labeled "EPD (ohmic only)").

2.6.5 Total minimum energy consumption. The total minimum energy consumption is the sum of minimum ohmic

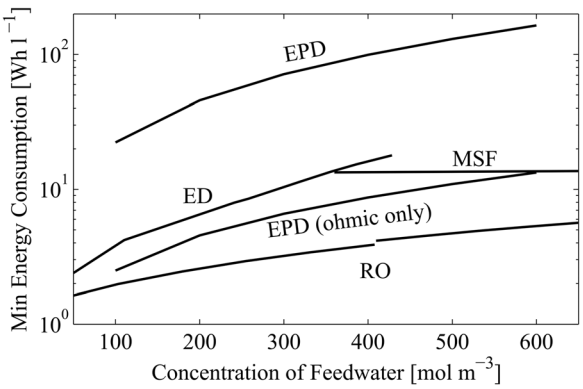

Fig. 4 Estimated minimum energy consumption per volume of product water for electrophoretic precipitative desalination (EPD) and typical energy consumption for common desalination processes including reverse osmosis (RO), electrodialysis (ED), and multi-stage flash distillation (MSF) at 70 °C. Energy consumption in EPD is roughly 90% from electrode reactions and 10% from ohmic losses. The electrode reactions are responsible for producing hydrogen, chlorine, and sodium hydroxide. These reactions are similar to those found in traditional processes that produce these products *via* electrolysis[25,26] and so consume roughly the same energy. In a co-generation application, the ohmic loss component of EPD is then the additional amount required for desalination. The ohmic component of the minimum required energy for EPD (the desalination component) is on par with the total energy consumption of other desalination methods. Energy consumption data for ED, MSF, and RO was digitized from Dilworth.[3]

energy consumption and electrode reactions energy consumption. For the former, we assume the average precipitate zone conductivity we measured in our experiments, 0.017 S m^{-1}. Electrode reactions constitute roughly 90% and ohmic losses constitute only 10% of the total energy. Electrode reactions are responsible for generation of hydrogen, chlorine, and sodium hydroxide, useful byproducts of this desalination method. If these products were to be produced at a seawater electrolysis hydrogen generation plant[25] or at a chlor-alkali process plant[26] these processes would require roughly the same energy input as the electrode reaction energy consumption in EPD. Driving ionic current through the feed water volume is responsible directly for the desalination and the additional ohmic losses. Since the desalination contribution of EPD is responsible for the ohmic loss, we may compare only the ohmic energy consumption of EPD to the total energy consumption of state-of-the-art desalination methods, which only desalinate water. Accordingly, we plot the total minimum energy consumption and the minimum ohmic only energy consumption of EPD in Fig. 4. We also compare this estimated minimum energy to typical values[3] for reverse osmosis (RO), electrodialysis (ED), and multi-stage flash distillation (MSF) at 70 °C. The total minimum energy consumption of EPD is naturally larger than typical energy consumption of ED, MSF and RO, as it is dominated by the energy consumed to produce hydrogen, chlorine, and sodium hydroxide. However, the component of EPD associated with ohmic energy consumption (responsible for desalination) is lower than the energy consumption of ED and MSF; and higher than that of RO. We point out that the membrane cost in operation of a typical RO plant can amount to as much as 30% of the energy cost in RO.[2] Taking this into account, the energy consumption of EPD over and above that required for useful electrode reactions may be generally on par with current state-of-the-art desalination methods.

3. Experimental

3.1 Materials and instrumentation

As a laboratory demonstration to study process efficacy and energy consumption, we performed EPD on sodium chloride solutions in simple, off-the-shelf optical white soda lime glass microfluidic chips (model NS12AZ, Caliper Life Sciences, Mountain View, CA). The chip channels are a simple cross geometry and are wet-etched to a 20 μm depth with a 50 μm mask width; the main channel is 72 mm long. We performed experiments in galvanostatic mode with a MATLAB computer-controlled Keithley 2410 high-voltage sourcemeter (Keithley Instruments, Cleveland, OH) with platinum wire electrodes (Sigma-Aldrich, St. Louis, MO). We observed the desalination process using an Olympus IX70 inverted fluorescence microscope equipped with 4× (NA of 0.16) and 10× (NA of 0.30) objectives (Olympus, Hauppauge, NY), a model XF129-2 filter cube (Omega Optical, Brattleboro, VT), and 365 nm UV LED (ThorLabs Newton, NJ) for illumination. Images were captured with a 12-bit 1300 by 1030 pixel charge-coupled device (CCD) camera (MicroMax RTE/CCD-1300Y/HS); controlled with WinView software, both from Roper Scientific, Trenton, NJ. Images were postprocessed with custom MATLAB scripts (R2010b, Mathworks, Natick, MA).

3.2 Experimental protocol

We prepared solutions of sodium chloride, sodium carbonate, and calcium carbonate (all from Sigma-Aldrich, St. Louis, MO) with deionized ultrafiltered water from Fischer Scientific (Pittsburgh, PA). To the sodium chloride solution we added 6-methoxy-*N*-(3-sulfopropyl)quinolinium (SPQ) (Invitrogen, Carlsbad, CA) and 1.3 MDa poly(vinylpyrrolidone) (PVP) (Arcos Organics Pittsburgh, PA) at a net concentration of 4 to 6.1 mol m^{-3} SPQ and 1% (w/v) PVP (for details see ESI†). SPQ and PVP are net electroneutral and thus do not contribute to electrical conductivity. We used PVP to suppress electroosmotic flow by dynamically coating the walls of the microchannel.[27,28] We performed EPD experiments in microchips with four wells. We filled the west, north, and south wells with sodium chloride and the east well with sodium carbonate (all same concentrations). We applied an electric field across the channel from west to east (see Fig. 1) using the sourcemeter in galvanostatic mode and measured voltage and recorded images of the anion exchange interface with the CCD camera. When the interface reached the west well, we turned off the current and vacuumed the west well, and immediately filled it with calcium chloride. We again applied electric field from west to east (see Fig. 1) while recording voltage and imaging. At the end of each experiment, we flushed the chip sequentially with hydrochloric acid, sodium hydroxide, and deionized water to prepare for the next experiment. We describe the experimental conditions in more detail in Section S10 of the ESI.†

3.3 Visualization and concentration quantification with the fluorescent ion indicator

We visualized the ion concentration in each zone with SPQ dye. SPQ is an ion sensitive net neutral fluorescent dye[28] which we used to visualize the carbonate and chloride zones and quantify zone anion concentration. SPQ dye responds to ions *via* diffusion limited collisional quenching.[28] It is net neutral and thus does not migrate due to an electric field. Its florescence intensity in the presence of an anion species is given by the Stern–Volmer equation:

$$\frac{F_0}{F} = 1 + K_{Q,i}[c_i], \tag{17}$$

where F_0 is the fluorescence intensity in the absence of quenchers, F is the fluorescence intensity in the presence of the quenching ion, c_i is the concentration of the quenching species i (the anion), and $K_{Q,i}$ is the quenching constant.[28] $K_{Q,i}$ is specific to the combination of florescent indicator, quenching anion species, and zone pH.[28] Thus fluorescence intensity of the zone is inversely proportional to the product of the quenching constant and the concentration of the anion of interest. Fluorescence of SPQ is quenched strongly in the presence of chloride ions ($K_{Q,Cl^-} = 107\ M^{-1}$) and to a lesser extent in the presence of carbonate ions $K_{Q,CO_3^{2-}} = 25\ M^{-1}$). We obtained the quenching constants by fitting eqn (17) with SPQ florescence at seven different concentrations of the respective quenching ions (for details see ESI†). We used the differential quenching to measure the concentration of carbonate in the sodium carbonate (trailing) zone, from known concentration of chloride in the sodium chloride zone and SPQ fluorescence in both zones:

$$c_{CO_3^{2-},Na^+/\overline{H_2CO_3}} = \frac{1}{K_{Q,CO_3^{2-}}}\left(\frac{F_{Cl^-,NaCl}}{F_{CO_3^{2-},Na^+/\overline{H_2CO_3}}}(1 + K_{Q,Cl^-}c_{Cl^-,NaCl}) - 1\right). \tag{18}$$

4. Results and discussion

We describe experiments that demonstrate the method's ability to desalinate water, and confirm trends for ohmic energy consumption and rate of desalination. We visualized the dynamics of ion zones and quantified interface velocities. We also desalinated sodium chloride solutions and measured the conductivity of the product water. To measure the ohmic energy consumption of the method, we measured the electrical energy consumption during desalination experiments.

4.1 Experimental demonstration of the concept

We observed and quantified ion concentrations with SPQ dye, observed precipitation with white light illumination, and measured the *I–V* characteristics of the process. In Fig. 5a and 5b we show spatio-temporal image data of the anion exchange and cation exchange visualized with SPQ dye. We plot the cross-sectional area-averaged intensity of SPQ fluorescence in the channel *versus* distance along the channel, x, and time, t. For the anion exchange experiment (Fig. 5a) we filled the channel and the west, north, and south well with 300 mol m^{-3} sodium chloride, 6.1 mol m^{-3} SPQ and 1% (w/v) PVP and the east well with 300 mol m^{-3} sodium carbonate solution with 1% (w/v) PVP. For the cation exchange experiment (Fig. 5b) we replaced the west well with 300 mol m^{-3} calcium chloride; the contents of the channel and the other wells remained from the anion exchange experiment. Both the cation exchange and the anion exchange experiments were performed at a constant current density of 3.3 kA m^{-2}.

The uniformity of fluorescence intensity within ion zones in Fig. 5a and 5b confirms the related assumptions that led to eqn (2). For anion exchange, the measured interface shock speed closely matches that predicted by the model. The measured concentration of carbonate ions are on the same order as those predicted by the model, and we attribute the difference to our uncertainty in the chloride-SPQ and carbonate-SPQ quenching constants.

For cation exchange we inferred the product zone composition from the measurement of the zone conductivity (see ESI†). The species concentration measurements (here we present only the calcium concentration, the species with the highest concentration) were bounded by those for the case of small and large precipitation-to-electromigration time scale ratios. This suggests that the time scales of the precipitation and electromigration are of comparable order. The measured product water concentration (0.8 mol m^{-3}) was an order of magnitude smaller than the maximum allowed concentration for fresh water (8 mol m^{-3}), thus demonstrating that we indeed desalinated the feed water.

We also measured the conductivity of the precipitate zone for desalination of 100 to 600 mol m^{-3} sodium chloride solutions. Each experiment was performed with 1% (w/v) PVP, and at concentrations of SPQ ranging between 4 and 6.1 mol m^{-3} and current densities ranging between 0.72 and 53 kA m^{-2} (for details see Section S10 of ESI†). We plot the measured conductivity of the precipitate zone as a function of feed water concentration in Fig. 3b. We again observe that the measured conductivity is bounded by that for the cases of small (solid lines) and large (dashed lines) precipitation-to-electromigration time scale ratios. We note that the product water conductivity very weakly depends on feed water concentration. Again the product water ion concentration is well below the maximum concentration allowed for fresh water. For the cation exchange, the observed interface speed was significantly greater than the predicted value. We hypothesize that we observed not the true interface speed but the interface speed plus the speed of the water due to a strong component of electroosmotic flow in the direction of the interface migration. This is consistent with electroosmotic flow in this type of glass channel, which is expected to be significant for both low conductivity and high electric field (the conditions in the precipitate zone).

In Fig. 5c we show calcium carbonate precipitate observed using transmitted white (room) light. The experiment was performed with 200 mol m^{-3} sodium chloride, 6.1 mol m^{-3} SPQ, 1% (w/v) PVP; 200 mol m^{-3} sodium carbonate, 1% (w/v) PVP; 200 mol m^{-3} calcium chloride, 1% (w/v) PVP, at a current density of 3.5 kA m^{-2}. Similar to the sodium carbonate–calcium carbonate zone interface, the precipitate interface remained sharp, and we believe this interface corresponded

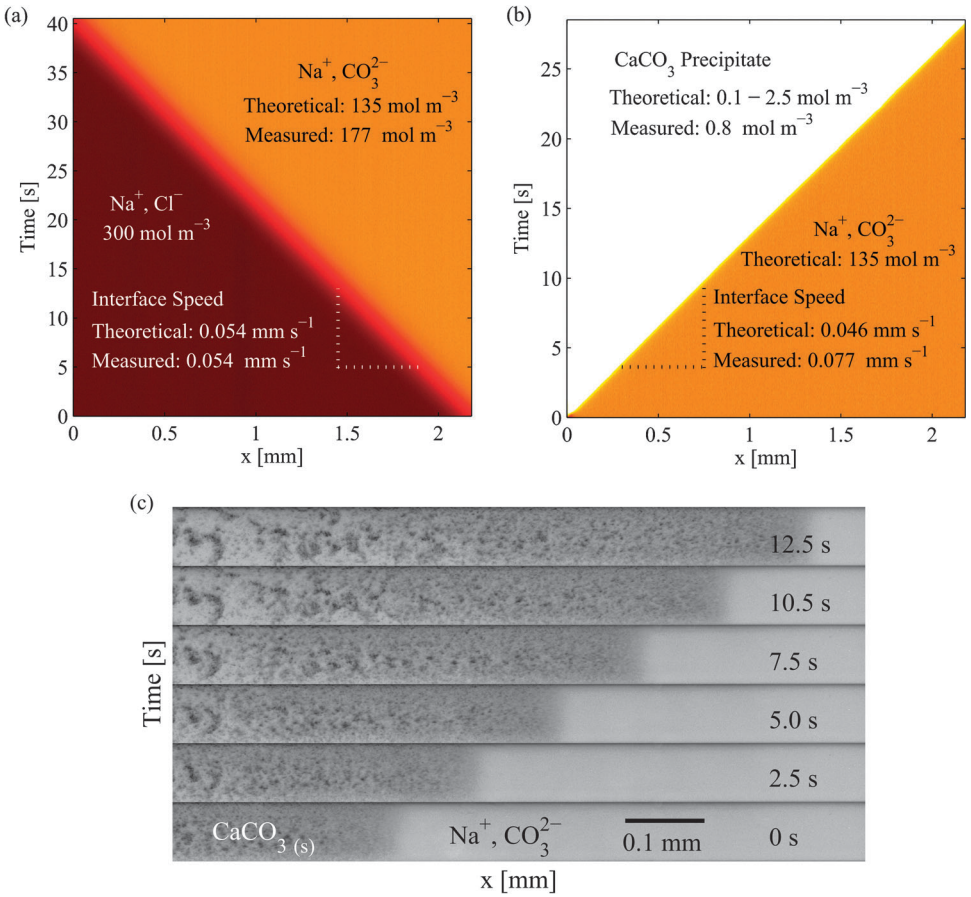

Fig. 5 Spatiotemporal visualization of electrophoretic precipitative desalination (EPD). Plots (a) and (b) show cross-sectional area-averaged intensity of SPQ fluorescence *versus* distance along the channel, x, and time, t, (c) shows six inverted intensity transmitted light microscope images of cation exchange at six times. In (a) we show the anion exchange step of EPD visualized with a net neutral fluorescent ion sensitive SPQ dye (6.1 mol m^{-3}). Under applied electric field (current density of 3.3 kA m^{-2}), the 300 mol m^{-3} chloride (dark zone) traveled leftward and was followed by sodium carbonate zone (bright zone). We calibrated the amount of quenching of SPQ fluorescence due to carbonate ions to estimate carbonate ion concentrations. The estimated concentration of carbonate ions roughly agrees with the carbonate concentration predicted by our model for the trailing zone. The measured interface speed agrees well with the theoretically predicted interface speed. (b) Cation exchange and precipitation of EPD visualized with SPQ. Under applied electric field (a current density of 3.3 kA m^{-2}), sodium zone (darker zone) traveled rightward, and was followed by calcium zone (brighter zone). The calcium reacted with counter-migrating carbonate ions to form calcium carbonate precipitate (not visible here due to fluorescence of SPQ). The ionic strength of the precipitate zone, inferred from channel electrical resistance, is of the same order as the predicted value. The measured interface speed is larger than that predicted theoretically, which we attribute to fairly strong electroosmotic flow. (c) Transmitted light microscope images of the calcium carbonate precipitate zone at six times during the cation exchange (precipitation) step. As carbonate ions counter migrated through the calcium zone, carbonate and calcium reacted to form calcium carbonate precipitate. Calcium carbonate precipitate formed with particles of the order of 10 μm. The interface between sodium and calcium (precipitate) zones remained sharp as predicted. We estimate that precipitates occupy less than 1% of channel volume.

to the sodium carbonate–calcium carbonate zone interface. The precipitate particles were roughly 10 μm in diameter. We observed the particles to grow behind the precipitate front, possibly due to Ostwald ripening.[29] Particles of 10 μm in diameter and larger can be easily settled out or filtered out using conventional low pressure filters, thus avoiding special membranes, and yielding desalinated water.

4.2 Ohmic energy consumption

To validate our model for ohmic energy consumption we measured energy required to desalinate 100 to 600 mol m^{-3} sodium chloride solutions as well as the interface width and speed. Each of these experiments was performed with 1% (w/v) PVP, and at concentrations of SPQ ranging between 4 and 6.1 mol m^{-3} and current densities ranging between 0.72 and 53 kA m^{-2} (for details see Section S10 of ESI†). We note our experimental geometry and conditions were very far from optimum. For example, our channels are very long and our current densities very large, resulting in channel-to-interface length scale ratios of order 10^3 and 10^6 for anion and cation exchange, respectively, and negligible electrode reactions compared to ohmic losses. Our geometry and conditions were chosen only to aid in visualization and to validate the basic model.

We compare the energy consumption measured in these experiments to that predicted by our models. We plot both in Fig. 4 as a function of feed water concentration from 100 to

600 mol m^{-3} sodium chloride. The energy consumption scaled by the product of channel volume, effective channel length, and current density for the cases of small (solid lines) and large (dashed lines) precipitation-to-migration time scale ratios bound the measured energy consumption.

5. Thoughts on implementation

5.1 Operation as a continuous process

We hypothesize that EPD can be operated as a batch process (such as with many chambers in parallel or in a porous medium) or as a continuous process. In a continuous process, streams of leading and trailing ion solutions would flow, for example, under applied pressure and side by side, while electric field would be applied transverse to the flow. The process would be analogous to continuous flow isotachophoresis, reviewed elsewhere.[30,31] The process can be imagined as discrete channels moving in the direction of hydrodynamic flow while the interface inside the channel moves with the electric field. We envision the need for two simultaneous, continuous flow apparatuses each performing anion exchange and cation exchange to complete the desalination process. We include further discussion of energy consumption in continuous free flow operation in Section S14 in ESI.†

5.2 Operation with reagent recycling

We hypothesize that the precipitate product can be recycled continuously to regenerate the replacement ion reagents. The electrode reaction products produced can also be recombined to produce (recover) energy. Thus, ideally, only feed water would enter the plant and brine and product water exit separately. For example, for a calcium carbonate system, sodium carbonate and calcium chloride can be regenerated using a modified Solvay process, described in detail elsewhere.[11] We provide some details of this proposed process in the ESI.†

6. Conclusion

We demonstrated a novel desalination method that operates at ambient temperature and pressure and employs no special membranes (a significant cost in RO[2] and ED[5] technologies). The method desalinates by electrophoretically replacing sodium and chloride ions in feed salt water with a cation and an anion which react and precipitate out. This precipitate is then removed, yielding low ionic strength product water. The process concurrently generates chlorine gas, hydrogen gas, and sodium hydroxide due to electrolysis.

We investigated the method's reagent consumption, permeate recovery ratio, and energy consumption. We hypothesize that reagents consumed in the desalination process can be regenerated using the commercially proven Solvay process. We estimate a permeate recovery ratio of 58% to 46% for feed water concentrations between 100 and 600 mol m^{-3} sodium chloride, values on par with RO. We developed a model for energy consumption and show that non-recoverable ohmic energy scales proportionally to current density and characteristic length of the system. We validated model predictions bounding ohmic energy consumption, desalination rate, and final conductivity with controlled experiments in a microfluidic chip. The experiments showed the efficacy of the desalination process.

We presented an estimate of the theoretical minimum energy required to desalinate. To minimize energy, we recommend decreasing current density and device length until the device length is about 5 times the characteristic widths of the interfaces between zones. In this limit, the additional energy required to desalinate over and above that necessary to generate hydrogen, chlorine, and sodium hydroxide *via* electrolysis was predicted to be 3 to 10 W h l^{-1}, which is on par with the energy consumed by state-of-the-art desalination methods. We therefore recommend the process may be feasible as part of a desalination-co-generation facility which generates fresh water, hydrogen gas, chlorine gas, and sodium hydroxide.

Acknowledgements

We gratefully acknowledge support from the National Science Foundation for a Graduate Research Fellowship for Viktor Shkolnikov and support from Mayfield Stanford Graduate Fellowship and a Kodak Fellowship for Supreet S. Bahga. This work was supported by National Science Foundation grant CBET-0967600-000.

References

1 S. Bernstein, ed. A. Marshall, United Nations Population Fund, 2001.
2 L. F. Greenlee, D. F. Lawler, B. D. Freeman, B. Marrot and P. Moulin, *Water Res.*, 2009, **43**, 2317–2348.
3 R. L. Dilworth, *Water Desalination*, Headquarters, Department of the Army, Washington D.C., USA, 1986.
4 M. A. Shannon, P. W. Bohn, M. Elimelech, J. G. Georgiadis, B. J. Marinas and A. M. Mayes, *Nature*, 2008, **452**, 301–310.
5 H. Strathmann, *Desalination*, 2010, **264**, 268–288.
6 P. B. Stewart, *Saline Water Conversion*, American Chemical Society, 1960, vol. 27, ch. 18, pp. 178–191.
7 D. E. Weiss, *Desalination*, 1966, **1**, 107–128.
8 J. D. Pless, M. L. F. Philips, J. A. Voigt, D. Moore, M. Axness, J. L. Krumhansl and T. M. Nenoff, *Ind. Eng. Chem. Res.*, 2006, **45**, 4752–4756.
9 A. E. Ghaly and M. Verma, *Am. J. Environ. Sci.*, 2008, **4**, 388–396.
10 A. R. Glueck, *Desalination*, 1968, **4**, 32–37.
11 J. J. McKetta, *Encyclopedia of Chemical Processing and Design: Slurry Systems, Instrumentation to Solid-Liquid Separation*, M. Dekker, 1995.
12 F. M. Everaerts, J. L. Beckers and T. P. E. M. Verheggen, *Isotachophoresis: Theory, Instrumentation, and Applications*, Elsevier, Amsterdam, New York, 1976.
13 P. Bocek, *Analytical Isotachophoresis*, VCH, Weinheim, Cambridge, 1987.
14 D. H. Marks, M. Balaban, B. A. Falagan, J. G. Jacangelo, K. L. Jones, W. J. Koros, J. J. Letey, T. M. Pankratz, R. H. Sakaji, C. D. Turner and M. Wilf, *Review of the Desalination and Water Purification Technology Roadmap*, The National Academies Press, Washington, D.C., 2004.
15 J. H. Masliyah and S. Bhattacharjee, *Electrokinetic and Colloid Transport Phenomena*, John Wiley & Sons, Hoboken, New Jersey, 2006.
16 P. K. Kundu and I. M. Cohen, *Fluid Mechanics*, Elsevier, Amsterdam, 2004.
17 A. Persat, R. D. Chambers and J. G. Santiago, *Lab Chip*, 2009, 9.
18 M. Bercovici, S. K. Lele and J. G. Santiago, *J. Chromatogr. A*, 2009, **1216**, 1008–1018.
19 S. S. Bahga, M. Bercovici and J. G. Santiago, *Electrophoresis*, 2010, **31**, 910–919.
20 J. P. Mericq, S. Laborie and C. Cabassud, *Water Res.*, 2010, **44**, 5260–5273.

21 A. J. Bard and L. R. Faulkner, *Electrochemical Methods: Fundamentals and Applications*, John Wiley & Sons, Inc., New York, 2000.
22 R. O'Hayre, S.-W. Cha, W. Colella and F. B. Prinz, *Fuel Cell Fundamentals*, Wiley, 2005.
23 D. A. MacInnes and L. G. Longsworth, *Chem. Rev.*, 1932, **9**, 171–230.
24 G. Garcia-Schwarz, M. Bercovici, L. A. Marshall and J. G. Santiago, *J. Fluid Mech.*, 2011, **679**, 455–475.
25 M. S. Casper, *Hydrogen Manufacture by Electrolysis, Thermal Decomposition, and Unusual Techniques*, Noyes Data Corp., Park Ridge, N.J, 1978.
26 P. Schmittinger, *Chlorine: Principles and Industrial Practice*, Wiley-VCH, Weinheim, 2000.
27 T. Kaneta, T. Ueda, K. Hata and I. Totaro, *J. Chromatogr. A*, 2006, **1106**, 52–55.
28 M. Vasseur, R. Frangne and F. Alvarado, *Am. J. Physiol.: Cell Physiol.*, 1993, **264**, C27–C31.
29 P. W. Voorhees, *J. Stat. Phys.*, 1985, **38**, 231–252.
30 T. Hirokawa and Y. Kiso, *J. Chromatogr. A*, 1994, **658**, 343–354.
31 D. Kohlheyer, J. C. T. Eijkel, A. van den Berg and R. B. M. Schasfoort, *Electrophoresis*, 2008, **29**, 977–993.